Hosseini Torshizi *et al.*
Cancer Nanotechnology (2024) 15:7
https://doi.org/10.1186/s12645-024-00246-6

RESEARCH

Open Access

Designing nanostructured lipid carriers modified with folate-conjugated chitosan for targeted delivery of osthole to HT-29 colon cancer cells: investigation of anticancer, antioxidant, and antibacterial activities

Ghazal Hosseini Torshizi[1], Masoud Homayouni Tabrizi[1*], Ehsan Karimi[1], Atefeh Younesi[1] and Zahra Larian[1]

*Correspondence:
Mhomayouni6@gmail.com

[1] Department of Biology, Mashhad Branch, Islamic Azad University, Mashhad, Iran

Abstract

The present study proposed to design nanostructured lipid carriers (NLC) coated with chitosan (CS) conjugated folate (FA) for the targeted delivery of Osthole (OST) to the HT-29 colon cancer cell line and improve its anticancer capability. To assess the physicochemical characteristics of OST-loaded NLC decorated with CS-conjugated FA (OST-NCF-NPS), several techniques, including DLS, SEM, and FTIR, were applied. After determining the encapsulation efficiency of OST in CSFA-modified NLC-NPs, an MTT test was conducted to evaluate the cytotoxic effects of this nano platform on the HT-29 cancer cell line in comparison to normal HFF cells. Possible mechanisms of apoptosis in cancer cells treated with OST-NCF-NPs were examined using qPCR, flow cytometry, and AO/PI fluorescent staining methods. Moreover, the antioxidant capacity of these biosynthesized nanocarriers was determined using ABTS and DPPH methods, and their antibacterial potential was measured through disk diffusion, MIC, and MBC assays. According to the findings, OST-NCF-NPS had the ideal average size of 179.19 nm, low polydispersity (PI = 0.23), acceptable physical stability (ζ-potential = + 18.99 mV), and high entrapment efficiency (83.5%). The MTT data demonstrated the selective cytotoxicity of NPs toward cancerous cells compared to normal cells. Cell cycle and Annexin V/Propidium Iodide (AnV/PI) analysis indicated that OST-NCF-NPs increased the sub-G1 population and AnV/PI-positive cells. The occurrence of programmed cell death in the treated cells was also verified by altered expression of proapoptotic (BAX and caspase-3) and antiapoptotic (Bcl-2) genes. Furthermore, the NPs exhibited strong antibacterial activity, particularly against gram-negative bacteria, and high antioxidant effects in reducing ABTS and DPPH-free radicals.

Keywords: Nanotechnology, Nanocarriers, Nanostructure lipid carriers, Colon cancer, Osthole, Chitosan, Apoptosis, Antioxidant

Graphical Abstract

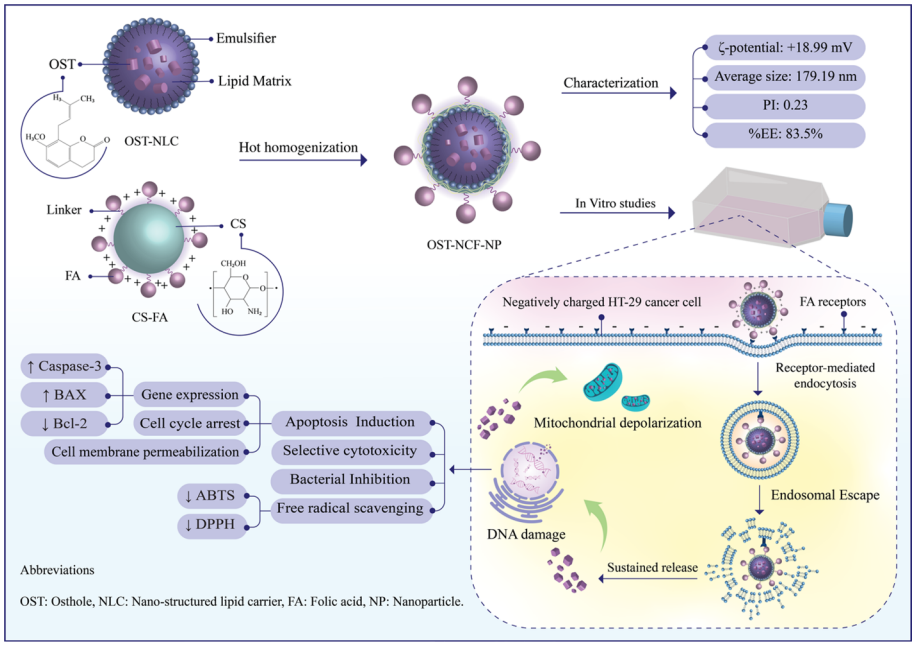

Introduction

Colorectal cancer is a major public health concern in both developed and developing nations, ranking third in terms of incidence rate among tumor-causing diseases and second among the causes of cancer-related mortality (Al-Joufi et al. 2022). The global burden of this malignancy is expected to escalate by 2030, resulting in more than 2.2 million newly diagnosed cases and over 1.1 million annual deaths (Rawla et al. 2019). Thus, it is crucial to introduce new preventive strategies to improve existing therapies and address this important health issue (Ruman et al. 2021). Natural products encompass a vast array of substances produced by living organisms, characterized by high structural diversity and low molecular weight. These compounds, whether naturally occurring or synthetically modified, have been employed as cancer chemotherapy agents, yielding significant results (Kinghorn et al. 2009). Osthole (OST), a biologically active coumarin compound found in the *Cnidium monnieri* plant (Zhang 2015), has been shown to possess potent antiproliferative properties and can induce apoptosis in multiple types of tumor cells in numerous studies (Su et al. 2019; Liang et al. 2020; Zhou et al. 2021). Moreover, it has been observed that OST can inhibit the metastatic spread of cancer cells by preventing their migration and invasion, making it a promising candidate for cancer treatment (Zhang 2015). However, the compound's clinical application faces significant challenges attributable to its water insolubility and low absorption, which consequently results in suboptimal bioavailability and efficacy. Therefore, its potential as a cancer treatment is limited, and alternative delivery strategies are necessary (Kulkarni et al. 2017). Utilizing nanoparticles (NPs) as drug delivery systems appears to be a promising tool to

overcome most of the limitations of current chemotherapeutic drugs. NPs are typically several hundred nanometers in size and can offer a new approach to improving cancer treatment by enhancing drug targeting, reducing toxicity, and improving localized drug efficacy, leading to better therapeutic results (Kemp and Kwon 2021; Rodenak-Kladniew et al. 2021). Therapeutic nano-delivery systems have shown multiple positive impacts over conventional cancer therapies due to their remarkable characteristics, such as enhanced permeability and retention, reduced toxic effects, and sustained drug release, leading to improved cellular uptake and delivery (Akinyelu and Singh 2019). Among them, lipidic nanocarriers have attracted a great deal of attention. These particles are categorized as solid lipid nanoparticles (SLNs) and nanostructured lipid carriers (NLCs) based on their composition. In NLCs, a small portion of liquid lipids is incorporated between solid lipids to facilitate the loading of active agents inside the nanocarrier (Dasineh et al. 2021). Due to the addition of liquid lipids to the solid lipid matrix, the lipidic core of these particles becomes less organized, resulting in a greater drug loading capacity, enhanced kinetic profiles, and prevention of drug expulsion during storage (Rodenak-Kladniew et al. 2021). Previous studies have reported the effectiveness of NLC-based delivery systems for transporting hydrophobic compounds to target cancer cells (Yostawonkul et al. 2017; Fernandes et al. 2018; Selvaraj and Yoo 2019). Modification of lipid nanosystems by coating their surface with polymers is a well-known strategy to improve the bioavailability of poorly soluble drugs (Dasineh et al. 2021). Chitosan (CS), a linear polycationic heteropolysaccharide, has found widespread use in various pharmaceutical and materials applications due to its abundance, low production cost, biodegradability, biocompatibility, renewability, and non-toxic nature (Agarwal et al. 2018). The positively charged amine groups of CS can interact electrostatically with the negatively charged surface of NLCs, leading to a change in surface charge from negative to positive. This alteration facilitates the active delivery of CS-modified carriers and increases their affinity for cancer cells with negative surface charges, playing an effective role in drug delivery to the target cells (Agarwal et al. 2018). On the other hand, specific receptors for certain ligands are often overexpressed in malignant cells. Formulating the surface of carriers with these ligands could increase their binding affinity to cancer cells and improve their uptake through the relevant receptors (Dhas et al. 2015). The expression of folate receptors is 100–300 times higher in colon cancer cells compared to normal cells (Ruman et al. 2021). Therefore, folate (FA) can serve as a binding ligand with high affinity to the surface of cancer cells and enter them through the receptor-mediated endocytosis pathway, enabling the targeted delivery of anticancer drugs (Yang et al. 2013). Several reports have demonstrated that FA-decorated CS can enhance the intracellular delivery of anti-cancer agents in cells overexpressing the folate receptor (Li et al. 2011; Soe et al. 2019; Khan, et al. 2020). Working on this rationale, the hypothesis of the present study was to design a nano-platform that would facilitate the targeted delivery of OST. The initial strategy involved the synthesis of OST-loaded NLC-NPs, followed by surface modification with CS-NPs conjugated with FA moieties, which produced the novel OST-NCF-NPs delivery system. The formulated NPs were then characterized in terms of the amount of entrapped OST and particle physicochemical properties. Upon confirming the successful formation of the NPs, the system's cytotoxic, apoptotic, antioxidant, and antibacterial activities were examined.

Experimental design and procedures

Materials

The substances used for encapsulation were purchased from Sigma–Aldrich and included glyceryl monostearate, oleic acid, tween 80, lecithin, low molecular weight chitosan (CS), folate (FA), 1-ethyl-3-(3-dimethyl aminopropyl) carbodiimide (EDC), and N-hydroxysuccinimide (NHS). Additionally, Sigma-Aldrich supplied the following: 3-(4,5-dimethylthiazol-2-yl)-2,5- diphenyltetrazolium bromide (MTT), dimethyl sulfoxide (DMSO), phosphate-buffered saline (PBS) tablets, Acridine orange (AO), Propidium Iodide (PI), Annexin V (AnV) and trypsin. The antioxidant assay required 2,2-diphenyl 1-picrylhydrazyl (DPPH), 2, 2′-azinobis-3-ethyl benzothiazole-6-sulfonic acid (ABTS), and ethanol, which were acquired from Merck. Materials utilized for cell cultures such as fetal bovine serum (FBS), penicillin, streptomycin, and DMEM and RPMI cell culture medium, were met from Gibco. The cell bank of the Ferdowsi College University of Mashhad provided human foreskin fibroblasts (HFF) and human colorectal adenocarcinoma (HT-29) for the study.

Preparation of OST-NLC

To prepare OST-loaded NLC, 50 mg of insoluble OST was dispersed in the lipid phase consisting of glyceryl monostearate as a solid matrix, 100 mL of oleic acid as a liquid matrix (0.89 *g*/mL), and lecithin (200 mg/mL) at 80 ℃. Meanwhile, an aqueous emulsifier phase was prepared by dissolving 40 mL of Tween 80 as a non-ionic surfactant with 60 mL of deionized distilled water at the same temperature. The lipid phase was poured dropwise into the aqueous phase under high-shear homogenization using an ultrasound probe sonicator system at 80 ℃ (15 min sonicating at 310 Watt, 8′′ On 2′′ Off). The homogenized suspension was stirred for 24 h at room temperature and subsequently centrifuged (Baek et al. 2015).

Preparation of CS-FA

The formation of the CS-FA derivative occurs through the activation of the carboxyl group of FA, which then undergoes a covalently binds with the primary amino group of CS leading to the formation of the conjugation (Ojeda-Hernández et al. 2022). For this, 20 mg of FA was completely dissolved in 50 mL of DMSO solution, followed by the addition of NHS (100 mM) and EDC (100 mM) while stirring continuously for 1 h. The by-product (dicyclohexylurea) was subsequently filtered out (Bano et al. 2016). In the next step, the resulting mixture was slowly added dropwise to 50 mL of CS solution (in 1% acetic acid) with a pH of 4.7 under constant stirring for 24 h. To complete the process, the pH was brought to 9.0 by adding aqueous sodium hydroxide and dialysis with phosphate buffer and deionized distilled water. The resulting precipitate was then centrifuged, dialyzed, and lyophilized. To prevent FA from decomposing, all reactions were carried out in the absence of light (Naghibi Beidokhti et al. 2017; Li et al. 2016).

Fabrication of OST-NCF-NPs

To modify the surface of OST-NLC, the CSFA powder was solubilized in 1% acetic acid and added in fine drops to the OST-NLC-NPs dissolved in deionized distilled water. After 3 h of incubation with constant stirring, the formed particles's dispersion was centrifuged. The supernatant containing unencapsulated OST was decanted and used for evaluating the percentage of encapsulated OST and the obtained sediment was stored in the refrigerator for further biological studies.

Entrapment efficiency

The amount of free OST in OST-NCF-NPs was evaluated by an indirect absorbance method (Mathew et al. 2010). For this, 3 ml of the supernatant collected during the centrifugation in the previous section (Sect. "Fabrication of OST-NCF-NPs") was taken in a cuvette, and the absorbance value at 220 nm wavelength was recorded with a Techocomp UV1100 spectrophotometer using the supernatant of their corresponding blank NPs as a basic correction. Then, the absorption of different concentrations of OST dissolved in deionized distilled water measured, and its standard curve was plotted. Finally, the entrapment efficiency (EE%) was calculated according to the equation below:

$$\mathrm{EE\%} = \frac{\text{total amount of OST in the initial dispersion} - \text{free OST in the supernatant}}{\text{total amount of OST in the initial dispersion}} \times 100 \quad (1)$$

Characterization procedures

The particle size, hydrodynamic diameter (z-average), polydispersity index (PDI), and surface charge (ζ-potential) of OST-NCF-NPs were measured using dynamic light scattering (DLS) at a detection angle of 90° and 25°, by a Malvern ZetaSizer Nano ZS90. Samples (1 mg) were resuspended in deionized distilled water (10 mL) and sonicated before to measurements (Esfandiarpour-Boroujeni et al. 2017). The morphological behavior (shape and size) of OST-NCF-NPs was determined utilizing a Mira3 field emission scanning electron microscope (FESEM). To prepare samples for imaging, a few drops of the dispersed NPs were sprayed onto an aluminum foil. The water was then allowed to evaporate at room temperature. Before being examined under the microscope, the dry particles were coated with a conductive gold and magnified between 10,00 and 40,000 (Wang et al. 2015). To analyze the structure of NPs, a Fourier transform infrared (FTIR) spectroscopy was performed using a Bruker, Tensor 27 IR spectrophotometer in a wavenumber range of 400–4000 cm^{-1}. A hydraulic press was used to mix 1 mg of NPs with 200 mg of potassium bromide powder and form a compact pellet, which was placed in the sensor of the instrument for the spectrum recording (Janardhanam et al. 2020).

Cell culture

Since the HT-29 cell line was identified to be the most sensitive after evaluating the toxicity of the biosynthesized particles against various lines of cancer cells in comparison with control (HFF cells), it has been chosen as the cancerous model in this study to investigate the potential of the OST-NCF-NPs. To initiate the cell culture, a population density of HT-29 cancerous cells (~ 8×10^4 cells/cm2) and the HFF normal

control cell line were seeded in RPMI and DMEM cell culture media, respectively, supplemented with 10% FBS and 1% antibiotics. Subsequently, the cells were thoroughly examined under a sterile cabinet and then incubated at a temperature of 37 ℃ in an environment with 5% carbon dioxide and 95% humidity.

Cytotoxic activity of OST-NCF-NPs

By performing an MTT experiment under a dose-dependent treatment protocol, the toxic potential of the synthesized carrier system and its half-maximal inhibitory concentration (IC_{50}) for HT-29 and HFF cell lines were evaluated (Maji et al. 2014). The principle underlying this method involves the cleavage of the tetrazolium rings of the MTT component (light yellow) by mitochondrial succinate dehydrogenase, leading to the formation of formazan crystals (dark purple), indicating metabolically active cells (Yuan et al. 2010). To perform the study, an optical density ($\sim 5 \times 10^3$ cells/well) of each cell line was first seeded in an eight-column culture plate in three replicates ($N=3$), and the cells were allowed to proliferate undisturbed overnight. Next, the cultured cells were exposed to a range of doses of OST-NCF-NPs (31.2, 65.5, 125, 250, and 500 µg/mL) serially, with negative control groups having no NPs included in the experiment. After 48 h of incubation, the old medium was removed, fresh medium supplemented with MTT solution was added to the wells, and the cells were incubated for an additional 3 h. To solubilize the formed formazan crystals, a new medium containing DMSO replaced the previous one and was mixed vigorously for 10 min. Finally, using a Statfax-2100 ELISA microplate reader, the medium's absorbance was measured at 570 nm, and the percentage index of cell viability (CV%) was determined according to the following equation.

$$\mathrm{CV\%} = \frac{\text{OD of the test sample}}{\text{OD of the control sample}} \times 100 \tag{2}$$

Apoptotic activity of OST-NCF-NPs

Quantitative PCR assessments of apoptosis-related genes

To analyze the effects of OST-NCF-NPs on apoptosis-related genes, such as caspase-3, B-cell lymphoma-2 (Bcl-2), and Bcl-2-associated X protein (BAX), a real-time polymerase chain reaction (qPCR) was performed based on the protocol presented by Tabatabaein et al. (Tabatabaeain et al. 2022). The HT-29 cancer cells (1×10^6) were initially seeded in 25 cm^2 flasks ($N=3$) and allowed to incubate for 24 h. Following this, the cells were exposed to the IC_{50} concentrations obtained from the MTT assay (65 and 115 µg/mL) for 48 h. No treatment was performed in the culture flask of the control group. The treated cells were subjected to transcriptome extraction using the Norgen RNA purification kit, and their complementary DNA (cDNA) library was prepared using the Parstous reverse transcription kit according to the recommended instructions of the respective manufacturers. Table 1 displays the sequences of primers that were optimized for cDNA using AlleleID 6 software. The housekeeping gene, glyceraldehyde-3-phosphate dehydrogenase (GAPDH), was employed to standardize the target gene expression. A mixture of cDNA, specific primers, Amplicon SYBER

Green, and deionized distilled water was prepared with a final volume of 20 µL for the qPCR reaction, which was carried out in a Biorad CFX96 real-time thermal cycler. Finally, qPCR efficiency was calculated based on the standard curves.

Flow cytometry analysis of apoptosis

The potential effect of OST-NCF-NPs on alterations in cell cycle distribution and the induction rate of apoptosis in HT-29 cells was investigated using flow cytometry analysis. This widely used method in both research and clinical settings identifies cells and evaluates their properties based on light scattering and fluorescence emission by fluorescent dyes. For cell cycle analysis, logarithmic phase cells were plated in a 6-well culture dish for 24 h and exposed to different concentrations of OST-NCF-NPs obtained from the MTT assay (65 and 115 µg/mL). The untreated culture plates served as controls. After 2 days of incubation, the treatment medium was washed with 500 µL of PBS, and trypsin (300 µL) was used to detach the cells. The cell-containing suspension was centrifuged (6 min), and the cell sediment was mixed with 300 µL of PI dye (1 mg/5 mL PBS + 0.2% Triton X100) and kept on ice in the dark for 30 min. The cells were then assessed using a FACScan laser flow cytometry (Sabzichi et al. 2017). The exact apoptosis rate in HT-29-treated cells was quantified through the Annexin V/Propidium Iodide (AnV/PI) staining method described by Sarawat et al. with slight modifications (Saraswat et al. 2020). Treated HT-29 cells were washed twice with ice-cold PBS (500 µL), detached in the presence of trypsin (300 µL), and collected in separate microtubes as above. Control cells received no OST-NCF-NPs treatment. Post this, the cells (5 µL) were stained with 1 µL of AnV along with 1 µLof PI dyes and kept under dark conditions for 20 min before analysis with the flow cytometer.

Fluorescence microscopy-based viability assay

To examine apoptosis and differentiate between viable and non-viable cells, a test involving staining with AO/PI was conducted. This test is based on the emission of fluorescent colors in green and orange-red wavelengths, respectively (Liao et al. 2016). As a procedure similar to flow cytometry, cultured cells were subjected to various doses of OST-NCF-NPs (65 and 115 µg/mL) and moved to microtubes following the trypsinization process. The harvested cells (5 µL) were then combined with a nucleic acid-binding dye solution consisting of 1 µL of AO and 1 µl of PI in PBS and incubated for 5 min. The resulting mixture was placed on a slide and examined under an OLYMPUS fluorescence microscope.

Table 1 The primer sets of the forward and reverse sequences that used for amplifying the targeted genes

Genes	Forward	Reverse
Caspase-3	$^{5/}$CTGGACTGTGGCATTGAGAC$^{3/}$	$^{5/}$ACAAAGCGACTGGATGAA$^{3/}$
BAX	$^{5/}$TTTGCTTCAGGGTTTCATCCA$^{3/}$	$^{5/}$CTCCATACTGTCCAGTTCGT$^{3/}$
Bcl-2	$^{5/}$CAGATAGGCACCCAGGGTGAT$^{3/}$	$^{5/}$CATGTGTGTGGAGAGCGTCAAC$^{3/}$

Antioxidant activity of OST-NCF-NPs

To determine the antioxidant potential of OST-NCF-NPs, the absorbance values of two different free radicals, ABTS and DPPH, were assessed in the presence of these NPs ($N=3$) utilizing a UV1100-Techcomp UV–Vis spectrophotometer, as described previously (Lin et al. 2021). A solution of ABTS cation radicals was produced by combining ABTS (7 mM) and potassium persulfate (2.45 mM) in 5 mL of deionized distilled water and incubated for 16 h in the dark at room temperature. Subsequently, a mixture containing a diluted solution (with an absorbance of 0.70 ± 0.02 at 734 nm) and solutions with different concentrations of OST-NCF-NPs (500, 250, 125, 62.5, and 31.2 µg/mL) were prepared, and incubated at 37 ℃ in a dark environment for 40 min before measuring the absorbance values at 734 nm. To generate DPPH cation radicals, an ethanolic DPPH solution (2.4 mg in 38.4 mL ethanol) was prepared and then mixed in equal parts with varying concentrations of OST-NCF-NPs (500, 250, 125, 62.5, and 31.2 µg/mL) and stirred. The reaction solution was incubated under the same conditions as the ABTS assay, and the samples were subjected to absorbance measurement at 517 nm. To ensure accuracy, both assays were repeated thrice ($N=3$), and the control group was prepared by combining ABTS and DPPH with deionized distilled water. The antioxidant activity (AA %) of OST-NCF-NPs was determined using the formula given below.

$$\mathrm{AA\%} = \frac{\text{OD of the test sample} - \text{OD of the control sample}}{\text{OD of the test sample}} \times 100 \tag{3}$$

Antimicrobial potential of OST-NCF-NPs

To evaluate the efficacy of OST-NCF-NPs against both gram-negative and gram-positive bacteria, various procedures were employed, including the Kirby-Bauer disk diffusion, Minimum Inhibitory Concentration (MIC), and Minimum Bactericidal Concentration (MBC) assays, all performed in triplicate ($N=3$). The Kirby-Bauer disk diffusion assay was conducted by first preparing a bacterial suspension, which was then used to inoculate a Muller-Hinton agar plate with a sterile swab. After uniform distribution of bacterial culture on the agar surface, sterilized disks were immersed in 500 µg/mL of OST-NCF-NPs for 1 min, then implanted on the agar surface with standard distances. The size of the zone of inhibition surrounding each disk was measured in millimeters after 24 h of incubation at 37 ℃. The negative control was a sterile distilled water disk, while gentamicin was used as a positive control (Ajitha et al. 2014). The micro broth dilution technique was used to determine the MBC and MIC of OST-NCF-NPs. Based on the preliminary study results, OST-NCF-NPs in concentrations ranging from 0 to 500 µg/mL (0, 31.2, 62.5, 125, 250, and 500 µg/mL) were serially diluted in sterile MHA in each well of a 96-well microplate. Bacterial suspensions (100 µL) were inoculated into each well, and the microplate was incubated at 37 ℃ for 24 h. The lowest concentration of OST-NCF-NPs required to inhibit microbial growth was identified as the MIC. To assess microbial growth, the absorbance at 620 nm was measured before and after incubation using a spectrophotometer. To determine the MBC, 100 µL of the content from wells showing no growth was added to MHA culture media without OST-NCF-NPs and incubated at 37 ℃ for 24 h. After incubation, the plates were examined for growth, and the lowest concentration

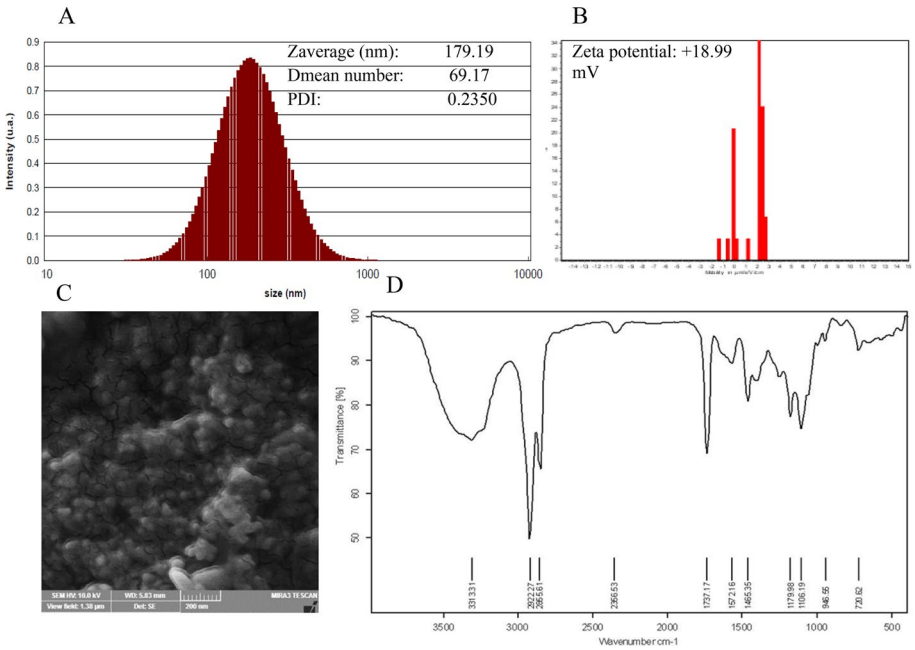

Fig. 1 Characterization data of OST-NCF-NPs. **A** Size dispersion by intensity. **B** Surface charge. **C** FESEM electron micrograph. **D** FTIR diagram. All measurements were performed in triplicate ($N = 3$). *OST-NCF-NPs* Nanostructured lipid carriers coated with chitosan conjugated folate nanoparticles containing Osthole, *DLS* Dynamic light scattering, *PDI* Polydispersity index, *FTIR* Fourier-transform infrared spectroscopy, *FESEM* Field Emission Scanning Electron Microscopy

of OST-NCF-NPs required to kill microorganisms was defined as MBC (Najafi et al. 2021). Chloramphenicol antibiotic powder was used as the control.

Data analysis

The statistical analysis was conducted by utilizing the SPSS software version 26. All the data were presented as the mean value ± standard deviation. To determine the statistical difference between the groups, the LSD test was applied after conducting a one-way analysis of variance (ANOVA). Any dissimilarities were acknowledged at the minimum significant level of less than 0.05.

Study results

Physicochemical characterization

The z-average of OST-NCF-NPs, a reliable index of the size of NPs, was measured at 179.19 nm, and the width of their diameter distribution, or the so-called PDI value was equal to 0.23 (Fig. 1A). Considering that the PDI value below 0.25 implies a fairly narrow size distribution, it can be said that the NPs have a monodisperse formulation (Lakshmi and Kumar 2010). To predict the long-term physical stability and release kinetics of OST-NCF-NPs, we measured their surface charge or ζ-potential, which was reported to be + 18.99 mV (Fig. 1B). Electrostatically stabilized nanosuspensions with pronounced ζ-potential values, typically around ± 30 mV, tend to accumulate

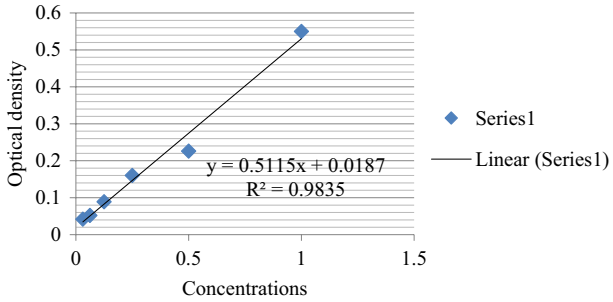

Fig. 2 The standard absorption diagram for various concentrations of OST was recorded at 220 nm. *OST* Osthole

less due to electrostatic repulsion between particles of the same charge, resulting in greater stability (Fan et al. 2014). However, we used both electrostatic (lecithin) and steric (Tween 80) stabilizers for the stabilization of NLCs. Hence, considering that further coating the NLCs with CS-FA can enhance their stability through surface layer hydration, the measured electric charge of + 18.99 mV is sufficient to prevent aggregation of this colloidal stabilized system (Tamjidi et al. 2013; Tamjidi et al. 2014). Three-dimensional FESEM micrographs revealed the presence of the spherical OST-NCF-NPs with a smooth surface and uniform size distribution of particles, which is in agreement with the defined size (Fig. 1C). The recorded FTIR diagram of OST-NCF-NPS provides basic information about the functional groups and possible chemical interactions between the different components (Fig. 1D) (Hashemi et al. 2020). The characteristic band at 3313.31 cm^{-1} is attributed to the combined effect of the OH and NH groups. Two distinct absorption peaks at 2922 cm^{-1} and 2855 cm^{-1} were observed due to C-H vibration. The wavelengths at 1737.17 cm^{-1} and 1572.16 cm^{-1} are typical of stretching due to the vibrations of C = O bonds. In addition, the bending vibration of C-H bonds can be seen at 1465.35 cm^{-1}. The presence of these specific peaks in the structure proves the successful encapsulation of OST in the carrier system and indicates that there is no chemical interaction between the components.

Entrapment efficiency

After conducting a calibration curve analysis of varied concentrations of OST, the results reveal a linear relationship with a slope of y = 0.5115x + 0.0187, corroborated by a high correlation coefficient of 0.9835 (Fig. 2). The amount of free OST was calculated by substituting the numbers into the linear relationship. Using the formula given in Sect. "Antioxidant Capacity", it was found that the entrapment of OST was 83.5%, showing the application potential of the delivery system.

Cell cytotoxicity assessment

A dose-dependent treatment plan was implemented to assess the cytotoxicity of OST-NCF-NPs using an MTT assay. The results revealed a significant reduction in the survival rate of HT-29 cancer cells with increasing doses of OST-NCF-NPs, and higher doses led to a greater decrease in viability (p-value < 0.001). Specifically, at a concentration of 31.2 µg/mL of OST-NCF-Ns, only 4% of cancer cells were inhibited.

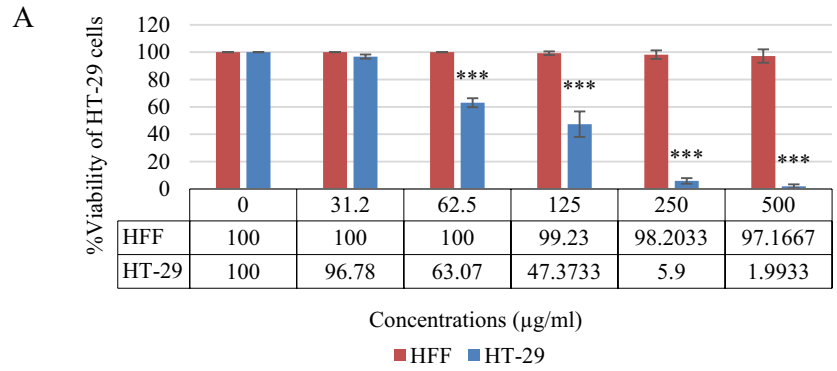

	0	31.2	62.5	125	250	500
HFF	100	100	100	99.23	98.2033	97.1667
HT-29	100	96.78	63.07	47.3733	5.9	1.9933

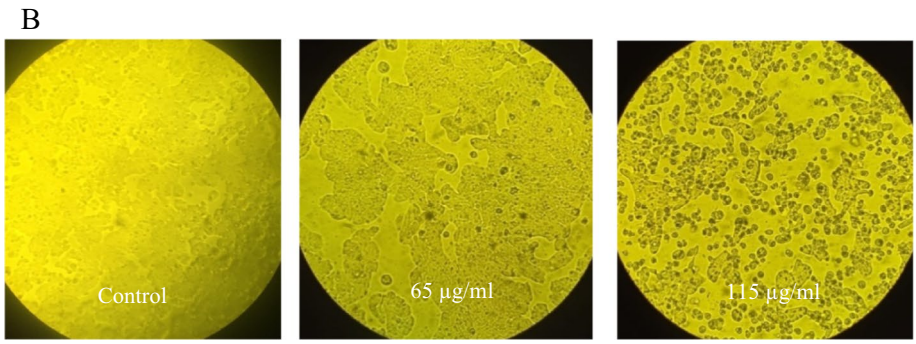

Fig. 3 Cytotoxic effects of OST-NCF-NPs. **A** Viability rate of HT-29 and HFF cell lines in comparison to control after exposure to various OST-NCF-NPs concentrations (31.2, 62.5, 125, 250, and 500 µg/mL). The treatment resulted in reduced cell viability, indicating the specific toxic effect of OST-NCF-NPs on the HT-29 cell line. **B** The morphology of treated HT-29 cancer cells under specific OST-NCF-NPs doses (65 and 115 µg/mL) compared to the untreated group. The *** denotes the level of a statistical significance level of < 0.001. ($N = 3$). OST-NCF-NPs: Nanostructured lipid carriers coated with chitosan conjugated folate nanoparticles containing Osthole; MTT: 3-(4,5-Dimethylthiazol-2-yl)-2,5-diphenyl tetrazolium bromide

However, as the treatment concentration increased to 62.5, 125, 250, and 500, the inhibition rate rose to 37%, 53%, 94%, and 98%, respectively (Fig. 3A). To determine the safe, non-toxic doses of OST-NCF-NPs, human HFF cells were chosen as a normal control cell line. No cytotoxic effects were observed on the normal HFF cells under the same treatment plan. This suggests that OST-NCF-NPs have a notable tissue-dependent cytotoxic effect on the HT-29 cell line, exhibiting a dual role of being toxic and non-toxic depending on the treatment doses. However, further studies with different cell lines are necessary to confirm its cell-dependent cytotoxicity. The IC_{50} value of OST-NCF-NPs, representing the half-maximal inhibitory concentration, was measured at 115.08 µg/mL, indicating that the toxic doses of this system on cancer cells are non-toxic and safe for normal cells. Two doses, 115 µg/mL and 65 µg/mL, were selected to evaluate the apoptosis-inducing properties of OST-NCF-NPs. Microscopic observation of the morphology of HT-29 cells treated with these doses revealed apoptotic bodies, indicating cell damage compared to the untreated group (Fig. 3B).

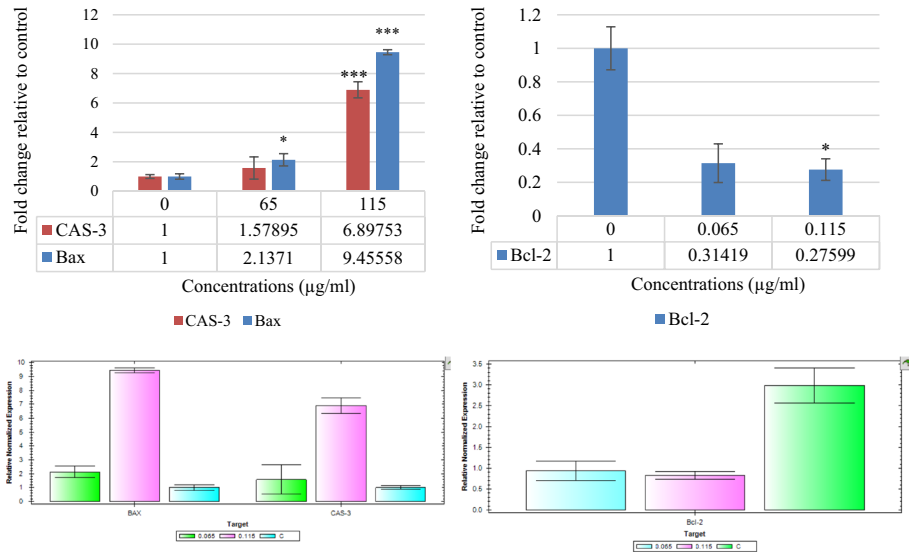

Fig. 4 Caspase-3, BAX, and Bcl-2 expression profiles in HT-29 cells following treatment with 65 and 115 µg/mL of OST-NCF-NPs in comparison to control. All reported values are the mean standard deviation derived from three separate experiments ($N = 3$). The '**' corresponds to the P-values of 0.01 and 0.01, respectively. *OST-NCF-NPs* Nanostructured lipid carriers coated with chitosan conjugated folate nanoparticles containing Osthole, *qPCR* Real-time PCR

Cell death type verification

qPCR assay for apoptotic-related gene expression analysis

The dose-dependent treatment of HT-29 cells with OST-NCF-NPs resulted in the upregulation of pro-apoptotic genes (BAX and caspase-3) and downregulation of the anti-apoptotic gene (Bcl-2) compared to the control group (Fig. 4). The overexpression of the caspase-3 gene was observed only at a concentration of 115 µg/mL (p-value < 0.001), while BAX gene expression increased substantially at both concentrations of 65 µg/mL (p-value < 0.05) and 115 µg/mL (p-value < 0.001). A comparison of anti-apoptotic Bcl-2 gene expression in treated and untreated cells showed a significant decrease in the mean concentration of the NPs (p-value < 0.05). These results imply that OST-NCF-NPs can induce cell death by triggering apoptotic pathways in the HT-29 cancer cell line.

Flow cytometry assay for cell death rate and cell cycle distribution analysis

To measure the exact apoptosis rate in HT-29 cells on exposure to OST-NCF-NPs, the apoptosis quantification was evaluated using the flow cytometric AnV/PI method. The analysis plots demonstrate the percentage distribution of necrotic cells (Q1: PI +, AnV-), late apoptotic cells (Q2: PI +, AnV +), early apoptotic cells (Q3: PI-, AnV +), and viable cells (Q4: PI-, AnV-). The total apoptosis was calculated as the sum of early and late apoptosis. The data indicated that the rate of apoptosis in HT-29 cells treated with 65 µg/mL and 125 µg/mL of OST-NCF-NPs increased by 25.9% (12.8% late apoptosis + 13.1% early apoptosis) and 25.11% (5.61% late apoptosis + 19.5% early apoptosis), respectively, compared to that in the control cells (Fig. 5A). These findings confirmed the induction of apoptosis in effective concentrations of OST-NCF-NPs.

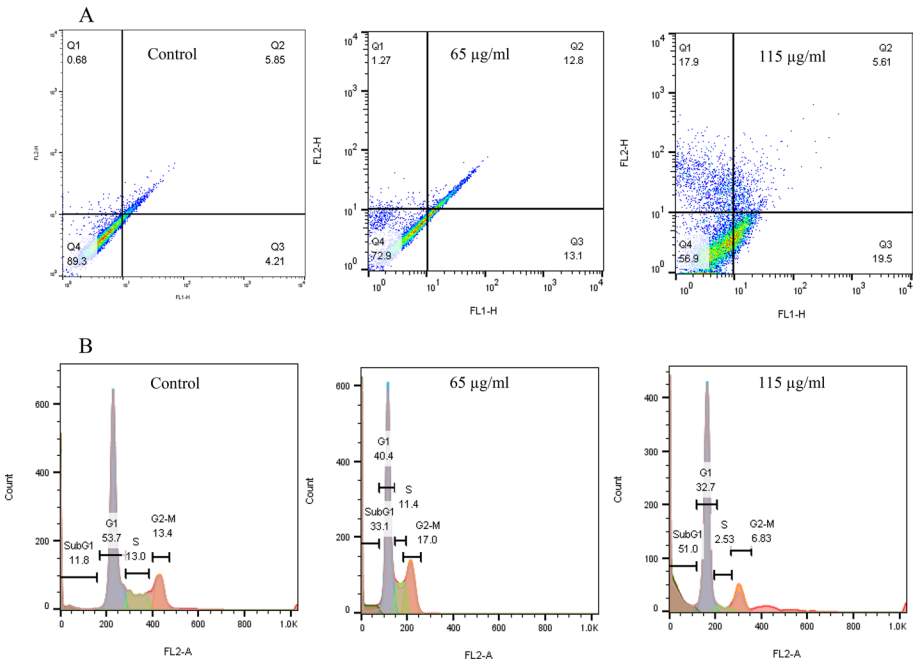

Fig. 5 The flow cytometric analysis data of the HT-29 cell line following treatment with 65 and 115 µg/ml of OST-NCF-NPs in comparison to the control. **A** The cell death rate of HT-29-treated cells. Treatment of HT-29 cells at a dose of 65 and 115 µg/mL for 24 h resulted in 25.59% and 25.11% apoptotic cells compared to untreated cells. Apoptotic cells (PI-, AnV +) were plotted as a percentage of the total cell population. The numbers represent the percentage of viable cells (Q4), early apoptotic cells (Q3), late apoptotic cells (Q2), and necrotic cells (Q1). B) Cell cycle distribution in HT-29-treated cells. Exposure of cells to OST-NCF-NPs increased the proportion of apoptotic cells as reflected by the sub-G1 peak. (Experiments were repeated in triplicate, Mean ± SD). *OST-NCF-NPs* Nanostructured lipid carriers coated with chitosan-conjugated folate nanoparticles containing Osthole, *AnV/PI* Annexin V/Propidium Iodide

To further verify the cell death type in HT-29-treated cells, the next step involved detecting cell cycle cessation through PI staining. DNA degradation during apoptosis makes the Sub-G1 peak an indicator in cell cycle analysis. The results demonstrated massive DNA degradation, as evidenced by an increase in the ratio of cells in the Sub-G1 phase of the cell cycle at the IC_{50} concentrations of OST-NCF-NPs compared to the control group (Fig. 5B). In HT-29 cells that received no treatment, the percentage of cells in the sub-G1 phase was 11.8%. After treatment with 65 µg/mL OST-NCF-NPs, the sub-G1 population climbed to 33.1%, and it further increased to 51% at a concentration of 115 µg/mL. This observation indicates increased apoptosis in these cells with an increase in the dosage of OST-NCF-NPs.

AO/PI Fluorescent staining

The findings of the AO/PI cell staining experiment reveal that the impact of OST-NCF-NPs on the viability and cell membrane integrity of the HT-29 cell line depends on the concentration of the treatment, exhibiting a dose-dependent manner. The untreated group manifested a colonized and healthy morphology, with all cells stained green, attributed to the AO dye's entrance into the plasma membrane of viable cells (Zahedifard et al. 2015). In contrast, the treated groups displayed a

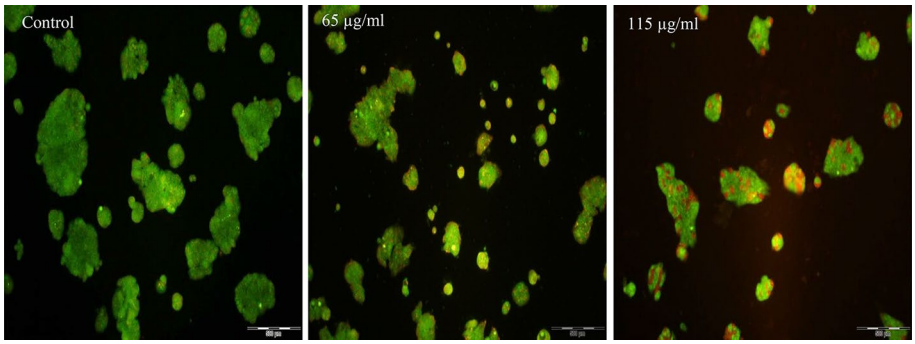

Fig. 6 Morphological changes of HT-29 cells during a 24-hour treatment plan with 65 and 115 µg/ml of OST-NCF-NPs compared with the untreated group confirmed the presence of apoptotic cells. In the control sample, cells exhibited a healthy, living state. However, the presence of yellow and orange/red cells indicated the occurrence of apoptosis. (N=3, Mean ± SD). OST-NCF- NPs: Nanostructured lipid carriers coated with chitosan-conjugated folate nanoparticles containing Osthole

significant reduction in green colonies, accompanied by a medley of cells turning yellow-orange. This transmutation is attributed to the PI dye's infiltration into the nuclear matter of damaged membranes, implying the presence of both early and late apoptotic cells (Fig. 6) (Alhajamee et al. 2022).

Antioxidant capacity

The data of the DPPH and ABTS tests demonstrate that OST-NCF-NPs possess a potent-free radical scavenging ability in a manner that is completely dependent on the applied dose (p-values < 0.001). It is worth noting that the inhibitory activity of OST-NCF-NPs was more pronounced than that of ABTS in targeting DPPH-free radicals (Fig. 7). In particular, the IC_{50} value, indicating the concentration of the compound required to inhibit half of the free radicals, was reported to be 198.61 µg/mL and 91.56 µg/mL in the ABTS and DPPH assays, respectively.

Antibacterial measurements

The antibacterial activity of OST-NCF-NPs against different gram-positive and gram-negative bacteria was analyzed through disk diffusion, MIC, and MBC assays and depicted in Table 2. According to the outcomes of the disk diffusion method, the inhibition zones for *Bacillus subtilis*, *Staphylococcus aureus*, *Escherichia coli*, and *Pseudomonas aeruginosa* were measured as 10 ± 0.82 and 13.3 ± 0.47 mm, 14 mm, and 16.7 ± 0.47 mm, respectively, signifying the potency of the NPs against these strains. Aditionally, OST-NCF-NPs exhibited a superior antibacterial effect on the Gram-negative *Pseudomonas aeruginosa* compared to the Gram-positive (Fig. 8). The results of the MIC and MBC assays showed that OST-NCF-NPs exhibited a notable killing effect on the gram-negative bacteria at 31.25 µg/mL of MIC and 62.5 µg/mL of MBC concentrations.

Discussion

The strategy of applying nanotechnology to plant extracts has made a remarkable contribution to treatment strategies, enabling the potentiation of the action of plant extracts, promoting sustained release of active constituents, reducing the required

dose, decreasing side effects, and improving activity (Bonifacio 2014). Ostole (OST), a coumarin compound, has been shown to exhibit antiproliferative properties such as promoting apoptosis, cell cycle arrest, inhibiting cell proliferation, triggering DNA damage, inducing the production of ROS as well as antibacterial activity against gram-negative and gram-positive bacteria (Sun et al. 2021). The chemical stability and bioavailability of this compound are compromised by its low solubility in aqueous solutions, which restricts its therapeutic uses (Wang et al. 2019). Nanoscale drug delivery systems have the potential to improve the biological activity of herbal compounds and overcome the problems associated with conventional plant-based medicines (Bonifacio 2014). Recent research has demonstrated a variety of nanocarriers, including polymeric and lipid-based cargos, can improve the anticancer effectiveness of several chemotherapeutic agents (Zhang and Misra 2019). Hence, this study focused on developing nanostructured lipid carriers (NLCs) decorated with chitosan (CS) conjugated folate to encapsulate OST (OST-NCF-NPs). The objective was to evaluate their biological performance in in vitro experiments. Nanocarriers must be formulated properly to protect the cargo from degradation, achieve prolonged circulation, avoid reticuloendothelial system uptake, and efficiently deliver to the target cells (Kemp and Kwon 2021). Therefore, the newly synthesized system underwent characterization of important factors such as size dimensions, PDI value, surface charge, surface chemistry, and shape using a variety of techniques. DLS measurements exhibited the formation of nanosized particles with an average diameter of 179.19 nm and a uniform size distribution (PDI = 0.23). In drug delivery approaches, the size of nanocarriers directly impacts their in vivo cellular uptake, excretion, and overall biological performance (Lakshmi and Kumar 2010). It has been suggested that particles with a diameter of 150–200 nm are favorable for passive targeting mechanisms, thus exhibiting a higher tendency to accumulate more efficiently in tumor microenvironments in vivo. Nanocarriers of this size can extravasate through vascular fenestrations of tumors and avoid filtration in the spleen, while still being large enough to prevent uptake in the liver (Aslan et al. 2013). Therefore, the evaluated size distribution for OST-NCF-NPs is convenient for biological applications. Another important parameter that affects the cellular uptake and stability degree of OST-NCF-NPs is the surface charge or the ζ-potential value which was measured by the DLS method at + 18.99 mV (Fig. 1A). The positively charged surface property of OST-NCF-NPs potentially increases their tendency to bind to cancer cells with a negative surface charge and enables them to interact with cell membranes more efficiently (Bashiri et al. 2020). Also, given that a surface charge of approximately ± 20 mV was reported to be sufficient for the formation of stable NLC-NP nanoparticles, OST-NCF-NPs can be considered stable (Truong et al. 2022; Sadeghzadeh et al. 2023a). The FESEM images showed special particles and the FTIR spectroscopy spectrum confirmed the compatibility among components of NPs (Fig. 1C). The EE% of OST-NCF-NPs was found to be 83.5% (Fig. 2), which is relatively high and consistent with previous studies on CS-coated NLCs (Ling et al. 2019; Lee et al. 2017). According to the physicochemical characteristics of the synthesized nanoparticles, it can be said that the formulation of OST-loaded NLC-modified CS-FA (OST-NCF-NPs) is a suitable carrier for effective drug delivery, especially with its positive surface charge that enhances their interaction with negative charge cancer cells. The synthesized drug delivery system was

tested for its potential cytotoxicity against colon cancer cells using the MTT method, and the results showed that they were selectively toxic to cancer cells because they significantly inhibited HT-29 cancer cells while showing no toxicity to HFF cells (Fig. 3). The targeted delivery of OST-NCF-NPs is likely due to the presence of FA, enabling the active targeting of these particles. This strategy relies on molecular recognition and leverages the overexpression of FA receptors on the surface of colon cancer cells. Once conjugated with FA receptors, OST-loaded nanocarriers are rapidly internalized into the cells through receptor-mediated endocytosis. Various FA-decorated polymer and liposomal nanocarriers have been developed to enhance drug uptake by cancer tissue (Li et al. 2011; Soe et al. 2019; Khan, et al. 2020). These experiments demonstrate that FA receptors can be effectively targeted for selective drug delivery by nanocarriers conjugated with FA. By utilizing FA-conjugated CS-NPs for the targeted delivery of ursolic acid to the MCF-7 breast cancer cell and taking advantage of the overexpressed FA receptors on the surface of these cells, Jin et al. observed enhanced cytotoxicity of this system in MCF-7 cells compared to ursolic acid alone. Furthermore, in vivo experiments indicated a reduction in breast cancer burden in the MCF-7 xenograft mouse model using this system (Jin et al. 2016). Likewise, Yang et al. reported that CS-conjugated FA could be an ideal vector for carrying 5-aminolaevulinic acid (5-ALA) to enhance the detection of colon cancer cells (Yang et al. 2010). Hence, it can be suggested that decorating the surface of NPs with FA is a safe and effective approach to diminish off-target effects and increase local drug concentrations. This can lead to the use of low doses in cancer treatment, which, in turn, will decrease undesirable side effects. Since our MTT assay and microscopic images were indicative of a reduction in the population of cancerous cells, for the next step, we aimed to verify the type of cell death by qPCR, fluorescent microscopy, and flow cytometry methods. The evasion of apoptosis, a highly regulated form of cell death, is a prominent hallmark of cancer that facilitates tumor development and allows neoplastic cells to survive beyond their intended lifespans. Tumor cells can acquire resistance to apoptosis through the expression of antiapoptotic proteins such as Bcl-2 or the downregulation of proapoptotic proteins such as BAX and caspases (Hassan, et al. 2014). Hence, the qPCR assay was utilized to examine the expression of genes associated with apoptosis, allowing us to gain a better understanding of the mechanisms of this programmed cell death. According to the qPCR results, the expression of BAX and caspase-3 genes was increased in HT-29 cells after treatment with OST-NCF-NPs, showing the pro-apoptotic potential of the synthesized particles (Fig. 4). This supports other mechanistic explorations on the apoptotic effects of NLCs and CS-coated NLCs, in which boosted levels of caspase-3 gene expression in MCF-7 cells were reported for Resveratrol-loaded NLCs and Resveratrol-loaded CS-NLCs (Elgizawy et al. 2021). The qPCR data also displayed a substantial decrease in Bcl-2 gene expression in HT-29 cancerous cells following OST-NCF-NPs treatment (Fig. 4). In line with this, Yostawonkul et al. documented the negative regulation of Bcl-2 by a CS-coated NLC-based vehicle containing alpha-mangosteen (Yostawonkul et al. 2017). Next, the quantification of apoptotic cells in the early and late stages was evaluated via annexin/PI assay. Since the apoptotic cells flip their inner side phosphatidylserine to the outer membrane, they can be recognized via binding of the protein annexin to this phospholipid. As our results illustrated, the percentage of

Table 2 The antibacterial activity of OST-NCF-NPs against pathogenic bacteria strains (*Bacillus subtilis*, *Staphylococcus aureus*, *Escherichia coli*, and *Pseudomonas aeruginosa*) in disk diffusion, MIC, and MBC

	Disk Diffusion		MIC		MBC	
	OST-NCF-NPs	Gentamicin	OST-NCF-NPs	Chloramphenicol	OST-NCF-NPs	Chloramphenicol
Bacillus subtilis (PTCC 1365)	10 ± 0.82 mm	22 mm	250 µg/mL	5 µg/mL	500 µg/mL	10 µg/mL
Staphylococcus aureus (ATCC 25923)	13.3 ± 0.47 mm	28.7 ± 0.47 mm	125 µg/mL	5 µg/mL	250 µg/mL	10 µg/mL
Escherichia coli (ATCC 25922)	14 mm	22.7 ± 0.47 mm	31.25 µg/mL	5 µg/mL	62.5 µg/mL	10 µg/mL
Pseudomonas aeruginosa (ATCC 9027)	16.7 ± 0.47 mm	21 mm	31.25 µg/mL	5 µg/mL	62.5 µg/mL	10 µg/mL

($N = 3$). *OST-NCF-NPs* Nanostructured lipid carriers coated with chitosan-conjugated folate nanoparticles containing Osthole, *MIC* The minimum inhibitory concentration, *MBC* Minimum bactericide concentration

apoptotic cells in the HT-29 treated cell line was elevated by about 25% in comparison with the control (Fig. 5A). Zhang et al. assessed the apoptotic induction of NLC-loaded Genistein (GEN-NLC) and NLC-coated CS containing GEN (GEN-NLC-CS) on HLE cells using annexin-based flow cytometry. Their results revealed a concentration-dependent apoptotic profile for both GEN-NLC and GEN-NLC-CS. However, the coated NLCs exhibited a higher percentage of apoptotic cells at each corresponding concentration level (Zhang et al. 2014). In addition to this, the results of the study by Geethakumari et al. on the population profile of FA-conjugated CS loaded with cytarabine in MCF-7 showed a significant increase in the percentage of apoptotic cells compared to cytarabine alone (Geethakumari et al. 2022). Apoptotic cell death was detected at the next level, demonstrating a significant and dose-dependent increase in the ratio of cells in the Sub-G1 phase of the cell cycle at OST-NCF-NPs concentrations compared to the control group (Fig. 5B). This result aligns with previous findings, wherein the treatment of MCF-7 with CS-FA-coated stylosin NLCs resulted in a significant augmentation of the sub-G1 population, indicative of small DNA fragments (Sadeghzadeh et al. 2023b). To further confirm that the observed sub-G1 phase resulting from OST-NCF-NPs treatment was due to its apoptosis-inducing characteristic, AO/PI staining was employed (Fig. 6). The results revealed an augmentation in the number of apoptotic cells and associated morphological changes indicative of apoptosis, which agrees with formly findings of Sadeghzadeh et al. (Sadeghzadeh et al. 2023a). Disruption of redox homeostasis contributes to multiple human diseases, including cancer. Resetting redox homeostasis with antioxidants presents a promising strategy to prevent tumorigenesis or inhibit cancer progression (Luo et al. 2022). Antioxidants are chemical

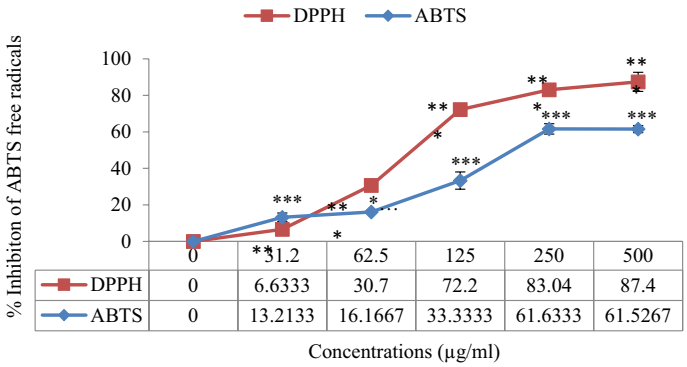

	0	31.2	62.5	125	250	500
DPPH	0	6.6333	30.7	72.2	83.04	87.4
ABTS	0	13.2133	16.1667	33.3333	61.6333	61.5267

Fig. 7 The free radical scavenging activity of OST-NCF-NPs, as determined by the ABTS and DPPH assays, was investigated across a range of concentrations (31.2, 62.5, 125, 250, and 500 µg/mL). The *** serves as a statistical indicator of the level of significance of the p-value of <0.001. Data represent the mean of 3 independent experiments. OST-NCF-NPs: Nanostructured lipid carriers coated with chitosan-conjugated folate nanoparticles containing Osthole; ABTS: 2, 2′-azinobis-3-ethyl benzothiazole-6- sulfonic acid; DPPH: 2,2-diphenyl 1-picrylhydrazyl

substances that neutralize free radicals by donating one of their electrons, preventing the free radical from taking electrons from other molecules (Singh et al. 2018). Our results indicate a significant concentration-dependent increase in ABTS and DPPH-free radical scavenging due to OST-NCF-NPs treatment (Fig. 7). Previous documentation reveals that OST exhibits an antioxidant effect by selectively inhibiting scavenging ROS and inhibiting lipid peroxidation (Ji et al. 2010). These studies suggest that OST can suppress the production of prostaglandin, nitric oxide, and malondialdehyde, while also decreasing the release of reactive oxygen metabolites (Liao et al. 2010; Rohmah et al. 2022). Therefore, it can be concluded that the antioxidant potential of this naturally occurring active compound is well-preserved within the developed nanocarriers. As shown by Rohmah et al. NLC-based systems efficiently encapsulate active compounds like OST (Rohmah et al. 2022). Further research demonstrates that OST-NCF-NPs exhibit antibacterial properties, with greater effectiveness against gram-negative than gram-positive bacteria (Table 2). Similar outcomes were reported in a recent study that evaluated the antioxidant potential and antibacterial activity of CS-lecithin NPs modified with PEG and folic acid (FA). The biosynthesized NPs showed substantial antioxidant and antibacterial effects against gram-negative bacterial strains (Hashemy 2023), comparable to those observed for OST-NCF-NPs.

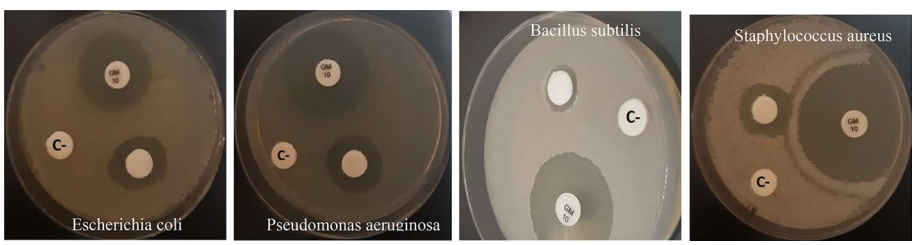

Fig. 8 Comparison of bacterial inhibition of OST-NCF-NPs and gentamicin antibiotic in Disk diffusion method. (N=3, Mean ± SD). OST-NCF-NPs: Nanostructured lipid carriers coated with chitosan-conjugated folate nanoparticles containing Osthole

Conclusion

The use of bioactive plant compounds as cancer therapeutics is widely known, yet conventional delivery techniques are constrained by their off-target side effects. Drug delivery to tumor sites is now more precise thanks to the development of nanomedicines and the manufacturing process and surface modifications have a great impact on the biological and physical properties of these drug delivery systems. In this research, we focused on developing a nanocarrier based on CS-FA-coated NLC to enhance the solubility, stability, and targeted delivery of OST to colon cancer cells. The synthesized nanocarrier exhibited a selective and stronger killer effect on cancer cells, including apoptosis via cycle arrest and activating the intrinsic apoptotic pathway at clinically relevant concentrations. In addition, the NPs demonstrated remarkable antioxidant and antibacterial activity. These results highlight the potential of OST-NCF-NPs as a viable therapeutic agent for colon cancer treatment. However, to fully establish the safety and efficiency of this NLC-modified system, additional in vitro experiments (e.g., 3D spheroids test, cellular uptake, drug release, hemolysis assay), in vivo studies, and additional colon cancer cell lines are necessary.

Abbreviations

OST	Osthole
NPs	Nanoparticles
NLC	Nanostructured lipid carriers
CS	Chitosan
FA	Folate
CSFA	Folate-conjugated Chitosan
OST-NCF-NPs	Folate-conjugated Chitosan-decorated Nanostructured Lipid Carriers containing Osthole
EDC	1-Ethyl-3-(3-dimethyl aminopropyl) carbodiimide
NHS	N-hydroxysuccinimide
MTT	3-(4,5-Dimethylthiazol-2-yl)-2,5-diphenyltetrazolium Bromide
DMSO	Dimethyl sulfoxide
PBS	Phosphate-buffered Saline
AO/PI	Acridine Orange/Propidium Iodide
AnV/PI	Annexin V/Propidium iodide
DPPH	2,2-Diphenyl-1-picrylhydrazyl
ABTS	2, 2′-Azinobis-3-ethyl benzothiazole-6-sulfonic Acid
FBS	Fetal bovine serum
HFF	Human foreskin fibroblasts
HT-29	Human colorectal adenocarcinoma
MIC	Minimum inhibitory concentration
MBC	Minimum bactericidal concentration
FTIR	Fourier-transform infrared spectroscopy
DLS	Dynamic light scattering
FESEM	Field emission scanning electron microscope
DMEM	Dulbecco's Modified Eagle Medium
PBS	Phosphate-Buffered Saline
RPMI	Roswell Park Memorial Institute Medium

Acknowledgements

This work was supported by, Islamic Azad University, Mashhad, Iran, and thus is appreciated by the author.

Author contributions

GHT, AY, and ZL: investigation, methodology and writing—original draft. MHT and EK: supervision, data curation, conceptualization software, validation and writing—reviewing.

Funding

This research was performed at personal expense in the laboratory of Islamic Azad University of Mashhad.

Availability of data and materials

The datasets used and/or analyzed during the current study are available from the corresponding author upon reasonable request.

Declarations

Ethics approval and consent to participate
All institutional and national guidelines for the care and use of laboratory animals were followed.

Consent for publication
Not applicable.

Competing interests
The authors declare that they have no competing interests.

Received: 27 March 2023 Accepted: 10 January 2024
Published online: 23 January 2024

References

Agarwal M et al (2018) Preparation of chitosan nanoparticles and their in-vitro characterization. Int J Life-Sci Sci Res 4(2):1713–1720
Ajitha B, Reddy YAK, Reddy PS (2014) Biogenic nano-scale silver particles by Tephrosia purpurea leaf extract and their inborn antimicrobial activity. Spectrochim Acta Part A Mol Biomol Spectrosc 121:164–172
Akinyelu J, Singh M (2019) Folate-tagged chitosan-functionalized gold nanoparticles for enhanced delivery of 5-fluorouracil to cancer cells. Appl Nanosci 9:7–17
Alhajamee M et al (2022) Co-encapsulation of curcumin and tamoxifen in lipid-chitosan hybrid nanoparticles for cancer therapy. Mater Technol 37(9):1183–1194
Al-Joufi FA et al (2022) Molecular pathogenesis of colorectal cancer with an emphasis on recent advances in biomarkers, as well as nanotechnology-based diagnostic and therapeutic approaches. Nanomaterials 12(1):169
Aslan B et al (2013) Nanotechnology in cancer therapy. J Drug Target 21(10):904–913
Baek J-S et al (2015) Tadalafil-loaded nanostructured lipid carriers using permeation enhancers. Int J Pharm 495(2):701–709
Bano S et al (2016) Paclitaxel loaded magnetic nanocomposites with folate modified chitosan/carboxymethyl surface; a vehicle for imaging and targeted drug delivery. Int J Pharm 513(1–2):554–563
Bashiri S et al (2020) Preparation and characterization of chitosan-coated nanostructured lipid carriers (CH-NLC) containing cinnamon essential oil for enriching milk and anti-oxidant activity. Lwt 119:108836
Bonifacio BV et al (2014) Nanotechnology-based drug delivery systems and herbal medicines: a review. Int J Nanomed 9:1–15
Dasineh S et al (2021) Tacrolimus-loaded chitosan-coated nanostructured lipid carriers: preparation, optimization and physicochemical characterization. Appl Nanosci 11:1169–1181
Dhas NL, Ige PP, Kudarha RR (2015) Design, optimization and in-vitro study of folic acid conjugated-chitosan functionalized PLGA nanoparticle for delivery of bicalutamide in prostate cancer. Powder Technol 283:234–245
Elgizawy HA, Ali AA, Hussein MA (2021) Resveratrol: isolation, and its nanostructured lipid carriers, inhibits cell proliferation, induces cell apoptosis in certain human cell lines carcinoma and exerts protective effect against paraquat-induced hepatotoxicity. J Med Food 24(1):89–100
Esfandiarpour-Boroujeni S et al (2017) Fabrication and study of curcumin loaded nanoparticles based on folate-chitosan for breast cancer therapy application. Carbohyd Polym 168:14–21
Fan H et al (2014) Development of a nanostructured lipid carrier formulation for increasing photo-stability and water solubility of phenylethyl resorcinol. Appl Surf Sci 288:193–200
Fernandes RS et al (2018) α-Tocopherol succinate loaded nano-structed lipid carriers improves antitumor activity of doxorubicin in breast cancer models in vivo. Biomed Pharmacother 103:1348–1354
Geethakumari D et al (2022) Folate functionalized chitosan nanoparticles as targeted delivery systems for improved anticancer efficiency of cytarabine in MCF-7 human breast cancer cell lines. Int J Biol Macromol 199:150–161
Hashemi FS et al (2020) Conjugated linoleic acid loaded nanostructured lipid carrier as a potential antioxidant nanocarrier for food applications. Food Sci Nutr 8(8):4185–4195
Hashemy SI et al (2023) PEGylated lecithin–chitosan–folic acid nanoparticles as nanocarriers of allicin for in vitro controlled release and anticancer effects. Appl Biochem Biotechnol 195:1–17
Hassan M et al (2014) Apoptosis and molecular targeting therapy in cancer. BioMed Res Int 2014:1
Janardhanam LSL et al (2020) Functionalized layer-by-layer assembled film with directional 5-fluorouracil release to target colon cancer. Mater Sci Eng, C 115:111118
Ji H-J et al (2010) Osthole improves chronic cerebral hypoperfusion induced cognitive deficits and neuronal damage in hippocampus. Eur J Pharmacol 636(1–3):96–101
Jin H et al (2016) Folate-chitosan nanoparticles loaded with ursolic acid confer anti-breast cancer activities in vitro and in vivo. Sci Rep 6(1):30782
Kemp JA, Kwon YJ (2021) Cancer nanotechnology: current status and perspectives. Nano Convergence 8(1):34
Khan MM et al (2020) Folate targeted lipid chitosan hybrid nanoparticles for enhanced anti-tumor efficacy nanomedicine: nanotechnology. Biol Med 28:102228
Kinghorn AD, Chin Y-W, Swanson SM (2009) Discovery of natural product anticancer agents from biodiverse organisms. Curr Opin Drug Discov Devel 12(2):189
Kulkarni AD et al (2017) N, N, N-Trimethyl chitosan: an advanced polymer with myriad of opportunities in nanomedicine. Carbohyd Polym 157:875–902
Lakshmi P, Kumar GA (2010) Nanosuspension technology: a review. Int J Pharm Sci 2(4):35–40

Lee SA et al (2017) Preparation of chitosan-coated nanostructured lipid carriers (CH-NLCs) to control iron delivery and their potential application to food beverage system. J Food Sci 82(4):904–912
Li P et al (2011) Synthesis and characterization of folate conjugated chitosan and cellular uptake of its nanoparticles in HT-29 cells. Carbohyd Res 346(6):801–806
Li L et al (2016) Preparation, in vitro and in vivo evaluation of bexarotene nanocrystals with surface modification by folate-chitosan conjugates. Drug Deliv 23(1):79–87
Liang J et al (2020) Osthole inhibits ovarian carcinoma cells through LC3-mediated autophagy and GSDME-dependent pyroptosis except for apoptosis. Eur J Pharmacol 874:172990
Liao P-C et al (2010) Osthole regulates inflammatory mediator expression through modulating NF-κB, mitogen-activated protein kinases, protein kinase C, and reactive oxygen species. J Agric Food Chem 58(19):10445–10451
Liao W et al (2016) Novel walnut peptide–selenium hybrids with enhanced anticancer synergism: facile synthesis and mechanistic investigation of anticancer activity. Int J Nanomed 11:1305
Lin D et al (2021) Comparison of apple polyphenol-gelatin binary complex and apple polyphenol-gelatin-pectin ternary complex: antioxidant and structural characterization. LWT 148:111740
Ling JTS, Roberts CJ, Billa N (2019) Antifungal and mucoadhesive properties of an orally administered chitosan-coated amphotericin B nanostructured lipid carrier (NLC). AAPS PharmSciTech 20(3):136
Luo M et al (2022) Antioxidant therapy in cancer: rationale and progress. Antioxidants 11(6):1128
Maji R et al (2014) Preparation and characterization of Tamoxifen citrate loaded nanoparticles for breast cancer therapy. Int J Nanomed 9:3107
Mathew ME et al (2010) Folate conjugated carboxymethyl chitosan–manganese doped zinc sulphide nanoparticles for targeted drug delivery and imaging of cancer cells. Carbohyd Polym 80(2):442–448
Naghibi Beidokhti HR et al (2017) Preparation, characterization, and optimization of folic acid-chitosan-methotrexate core-shell nanoparticles by box-behnken design for tumor-targeted drug delivery. AAPS PharmSciTech 18:115–129
Najafi M, Moghaddam MN, Yousefi E (2021) The effect of silver nanoparticles on pyocyanin production of Pseudomonas aeruginosa isolated from clinical specimens. Avic J Med Biotechnol 13(2):98
Ojeda-Hernández DD et al (2022) Chitosan-hydroxycinnamic acids conjugates: emerging biomaterials with rising applications in biomedicine. Int J Mol Sci 23(20):12473
Rawla P, Sunkara T, Barsouk A (2019) Epidemiology of colorectal cancer: incidence, mortality, survival, and risk factors. Gastroenterol Rev/przegląd Gastroenterol 14(2):89–103
Rodenak-Kladniew B et al (2021) Design of magnetic hybrid nanostructured lipid carriers containing 1, 8-cineole as delivery systems for anticancer drugs: Physicochemical and cytotoxic studies. Colloids Surf, B 202:111710
Rohmah M, Rahmadi A, Raharjo S (2022) Bioaccessibility and antioxidant activity of β-carotene loaded nanostructured lipid carrier (NLC) from binary mixtures of palm stearin and palm olein. Heliyon 8(2):e08913
Ruman U et al (2021) Synthesis and characterization of chitosan-based nanodelivery systems to enhance the anticancer effect of sorafenib drug in hepatocellular carcinoma and colorectal adenocarcinoma cells. Nanomaterials 11(2):497
Sabzichi M et al (2017) Vitamin D-loaded nanostructured lipid carrier (NLC): a new strategy for enhancing efficacy of doxorubicin in breast cancer treatment. Nutr Cancer 69(6):840–848
Sadeghzadeh F et al (2023a) Folic acid conjugated-chitosan modified nanostructured lipid carriers as promising carriers for delivery of Umbelliprenin to cancer cells: In vivo and in vitro. Eur Polymer J 186:111849
Sadeghzadeh F et al (2023b) Nanofabrication of PLGA-PEG-chitosan-folic acid systems for delivery of colchicine to HT-29 cancer cells. J Biomater Sci Polym Ed 34(1):1–17
Saraswat A et al (2020) Nanoformulation of PROteolysis TArgeting Chimera targeting 'undruggable'c-Myc for the treatment of pancreatic cancer. Nanomedicine 15(18):1761–1777
Selvaraj K, Yoo B-K (2019) Curcumin-loaded nanostructured lipid carrier modified with partially hydrolyzed ginsenoside. AAPS PharmSciTech 20:1–9
Singh K et al (2018) Antioxidants as precision weapons in war against cancer chemotherapy induced toxicity–Exploring the armoury of obscurity. Saudi Pharm J 26(2):177–190
Soe ZC et al (2019) Folate-targeted nanostructured chitosan/chondroitin sulfate complex carriers for enhanced delivery of bortezomib to colorectal cancer cells. Asian J Pharm Sci 14(1):40–51
Su J et al (2019) Osthole promotes the suppressive effects of cisplatin on NRF2 expression to prevent drug-resistant cervical cancer progression. Biochem Biophys Res Commun 514(2):510–517
Sun M, Sun M, Zhang J (2021) Osthole: An overview of its sources, biological activities, and modification development. Med Chem Res 30(10):1767–1794
Tabatabaeain SF, Karimi E, Hashemi M (2022) Satureja khuzistanica essential oil-loaded solid lipid nanoparticles modified with chitosan-folate: evaluation of encapsulation efficiency, cytotoxic and pro-apoptotic properties. Front Chem 10:904973
Tamjidi F et al (2013) Nanostructured lipid carriers (NLC): a potential delivery system for bioactive food molecules. Innov Food Sci Emerg Technol 19:29–43
Tamjidi F et al (2014) Design and characterization of astaxanthin-loaded nanostructured lipid carriers. Innov Food Sci Emerg Technol 26:366–374
Truong TH et al (2022) Chitosan-coated nanostructured lipid carriers for transdermal delivery of tetrahydrocurcumin for breast cancer therapy. Carbohyd Polym 288:119401
Wang W et al (2015) Poly (lactic acid)/chitosan hybrid nanoparticles for controlled release of anticancer drug. Mater Sci Eng, C 46:514–520
Wang R et al (2019) New insights into the binding mechanism between osthole and β-lactoglobulin: Spectroscopic, chemometrics and docking studies. Food Res Int 120:226–234
Yang S-J et al (2010) Folic acid-conjugated chitosan nanoparticles enhanced protoporphyrin IX accumulation in colorectal cancer cells. Bioconjug Chem 21(4):679–689
Yang KK et al (2013) Folate-modified–chitosan-coated liposomes for tumor-targeted drug delivery. J Mater Sci 48:1717–1728

Yostawonkul J et al (2017) Surface modification of nanostructure lipid carrier (NLC) by oleoyl-quaternized-chitosan as a mucoadhesive nanocarrier. Colloids Surf, B 149:301–311
Yuan Q, Hein S, Misra R (2010) New generation of chitosan-encapsulated ZnO quantum dots loaded with drug: synthesis, characterization and in vitro drug delivery response. Acta Biomater 6(7):2732–2739
Zahedifard M et al (2015) Synthesis, characterization and apoptotic activity of quinazolinone Schiff base derivatives toward MCF-7 cells via intrinsic and extrinsic apoptosis pathways. Sci Rep 5(1):1–17
Zhang J, Misra R (2019) Nanomaterials in microfluidics for disease diagnosis and therapy development. Mater Technol 34(2):92–116
Zhang W et al (2014) Enhanced cellular uptake and anti-proliferating effect of chitosan hydrochlorides modified genistein loaded NLC on human lens epithelial cells. Int J Pharm 471(1–2):118–126
Zhang Z-R et al (2015) Osthole: a review on its bioactivities, pharmacological properties, and potential as alternative medicine. Evid-Based Complement Altern Med 2015:1
Zhou X-H et al (2021) Osthole induces apoptosis of the HT-29 cells via endoplasmic reticulum stress and autophagy. Oncol Lett 22(4):1–9

Publisher's Note